

1 **Return flows from beaver ponds enhance floodplain-to-river metals exchange in**
2 **alluvial mountain catchments**

3
4
5 Martin A. Briggs^{1*}, mbriggs@usgs.gov

6 Chen Wang²

7 Frederick D. Day-Lewis¹

8 Ken Williams^{3,4}

9 Wenming Dong³

10 John W. Lane¹

11
12
13
14 ¹U.S. Geological Survey, Earth System Processes Division, Hydrogeophysics Branch, 11
15 Sherman Place, Unit 5015, Storrs, CT USA

16 ²Department of Earth and Environmental Sciences, Rutgers University, Newark, NJ USA

17 ³Lawrence Berkeley National Laboratory, Earth & Environmental Sciences Area, 1 Cyclotron,
18 Road, MS74R316C, Berkeley, CA USA

19 ⁴ Rocky Mountain Biological Lab, Gothic, CO USA

20

21

1

22 Draft resubmission to *Science of the Total Environment* (05/24/2019)

23 **Abstract**

24 River to floodplain hydrologic connectivity is strongly enhanced by beaver- (*Castor canadensis*)
25 engineered channel water diversions. The hydroecological impacts are wide ranging and
26 generally positive, however, the hydrogeochemical characteristics of beaver-induced flowpaths
27 have not been thoroughly examined. Using a suite of complementary ground- and drone-based
28 heat tracing and remote sensing methodology we characterized the physical template of beaver-
29 induced floodplain exchange for two alluvial mountain streams near Crested Butte, Colorado,
30 USA. A flowpath-oriented perspective to water quality sampling allowed characterization of the
31 chemical evolution of channel water diverted through floodplain beaver ponds and ultimately
32 back to the channel in ‘beaver pond return flows’. Return seepages were universally suboxic,
33 while ponds and surface return flows showed a range of oxygen concentration due to in-situ
34 photosynthesis and atmospheric mixing. Median concentrations of reduced metals: manganese
35 (Mn), iron (Fe), aluminum (Al), and arsenic (As) were substantially higher along beaver-induced
36 flowpaths than in geologically controlled seepages and upstream main channel locations. The
37 areal footprint of reduced return flow seepage flowpaths were imaged with surface
38 electromagnetic methods, indicating extensive zones of high-conductivity shallow groundwater
39 flowing back toward the main channels and emerging at relatively warm bank seepage zones
40 observed with infrared. Multiple-depth redox dynamics within one focused seepage zones
41 showed coupled variation over time, likely driven by observed changes in seepage rate that may
42 be driven by pond stage. High-resolution times series of dissolved Mn and Fe collected
43 downstream of the beaver-impacted reaches indicated seasonal dynamics in mixed river metal

44 concentrations. Al time series concentrations showed proportional change to Fe at the smaller
45 stream location, indicating chemically reduced flowpaths were sourcing Al to the channel.
46 Overall our results indicated beaver-induced floodplain exchanges create important, and perhaps
47 dominant, transport pathways for floodplain metals by expanding chemically-reduced zones
48 paired with strong advective exchange.

49

50

51 **Key words:** river; groundwater/surface water interactions; beaver; floodplain; drone; water
52 quality

53

54 **1. Introduction**

55 The concept of ‘river corridor’ science recognizes that the quality of flowing surface
56 waters is intrinsically linked to their contributing catchments through hydrologic connectivity,
57 including lower terrestrial hillslopes, floodplains, and riparian zones (Covino, 2017; Poole, 2010;
58 Vidon et al., 2010). Bidirectional river-floodplain exchange in particular can be critical to basin
59 water storage and nutrient transformation dynamics (Harvey and Gooseff, 2015), yet floodplain
60 hydrologic exchange flows are often driven primarily by episodic high-flow events (e.g. Sawyer
61 et al., 2014) or relatively slow-exchanging, long hyporheic flowpaths (Boano et al., 2014).
62 Beaver (*Castor canadensis*) disrupt these abiotic floodplain exchange drivers by actively
63 diverting large quantities of channel water laterally using an engineered series of dams,
64 impacting both wet and dry season floodplain connection (Westbrook et al., 2006). As humans
65 allow beaver to return to their extensive natural habitats across North America, the fundamental
66 dynamics of river corridor hydrologic connectivity are being strongly altered toward a template
67 of spatial ‘discontinuum’ and enhanced exchange (Burchsted et al., 2010). Much beaver-induced
68 floodplain disturbance is undoubtedly viewed as a net positive in the context of natural and
69 efficient watershed restoration. But as beaver ponds and seepage zones accompanying beaver
70 activity often exhibit suboxic to hypoxic conditions (Collen and Gibson, 2000), there is the
71 potential to mobilize large quantities of reduced metals and associated contaminants from
72 alluvial sediments to streams and rivers.

73 Beaver populations are steadily increasing in North America due to stricter trapping laws,
74 a general decline in trapping interest, passive and active conservation efforts, and a relative
75 absence of predators (Hood, 2011). In one sense, this rebound can be viewed as North American
76 watersheds returning to a natural, or pre-European settlement state one that is extensively

77 engineered by the beaver. Before European settlement the North American beaver population
78 numbered between 60-400 million individuals (Seton, 1929), and their dams and foraging
79 influenced almost every floodplain system from arid Mexico to the arctic tundra (Naiman et al.,
80 1988). After the arrival of significant numbers of Europeans in the early 1600's beaver
81 populations declined in response to extreme trapping until the animal was functionally extinct on
82 the continent by 1900. Before trapping began, most rivers in North America had extensive
83 beaver-induced floodplains and numerous wood snags that retained carbon and nutrients in the
84 headwaters. Evidence of the extensive effects on the riparian landscape of large historical
85 populations can still be seen hundreds of years later (Naiman et al., 1986).

86 Beaver construct dams across streams and wetlands to increase habitat favorable to their
87 basic needs of forage and protection. Impoundments can have a variety of influences on the
88 physical and biological characteristics of floodplain areas and riparian zones. Analogous to
89 anthropogenic dams, the combined effects of beaver dams is often a reduction in peak river
90 discharge, a smoothing of catchment outlet hydrograph (Ligon et al., 1995), and a general
91 increase in reach-scale water residence time (Jin et al., 2009). These moderated flow patterns can
92 stabilize the stream channel and decrease bed mobilization by reducing erosive forces, such as
93 shear stress on the stream bank and along the sediment-water interface. Storage of water behind
94 the dams can be an appreciable fraction of the catchment surficial water budget during dry
95 periods and often results in greater connection between riparian vegetation and the water table
96 throughout the year. An analysis of aerial photo mosaics from 1948 to 2002 from Central
97 Alberta, Canada indicated that the number of 'active' beaver lodges could explain greater than
98 80% of the variability in floodplain open water area through a number of wet and dry periods
99 (Hood and Bayley, 2008). However, the beaver-induced water storage story is complex. Some

100 studies have also suggested that the ecological effects of increased water storage may be negated
101 in part by amplification of the evaporative flux due to an increase in stream and floodplain
102 surface water area (Collen and Gibson, 2000). Recent work has indicated that beaver-induced
103 recharge of alluvial floodplains may not substantially increase late summer low-flows, in part
104 because much of this floodplain water may be trapped in low permeability soils and/or is simply
105 recently diverted channel water (Nash et al., 2018). However, flows returning to the channel
106 from reactive beaver-induced floodplain storage are likely to be important conduits of carbon
107 transport (Catalán et al., 2017) and nutrient transformation (Briggs et al., 2013; Wegener et al.,
108 2017) throughout the year.

109 The recent phenomena of encouraging beaver recolonization and the installation of
110 anthropogenic ‘beaver dam analogues’ in the context of stream restoration hopes to capitalize on
111 expected net positive hydrogeological and ecosystem impacts (Lautz et al., 2018; Pilliod et al.,
112 2018; Wohl et al., 2015). Natural and simulated dams can mitigate incised western channels by
113 increasing floodplain connection and riparian vegetation regrowth, which in turn positively
114 influences desirable recreational fish populations (Bouwes et al., 2016). The channel water
115 temperature response to beaver-induced floodplain connection is complicated and spatially
116 heterogeneous (Majerova et al., 2015), but it has been shown to moderate the warmest daily
117 temperatures and provide cool thermal refugia for stressed aquatic species in Oregon (Weber et
118 al., 2017). Benefits of beaver colonization that may outweigh complications to infrastructure
119 have even been recently recognized for urban drainages (Bailey et al., 2019). However, not all
120 impacts of natural and simulated beaver dams will be desirable to humans (Pilliod et al., 2018).
121 Negative impacts of result mainly from the raising of the water table adjacent to the stream,

122 flooding, impoundment of drainage systems, and the cutting of desirable vegetation (Collen and
123 Gibson, 2000).

124 Gradients in pH and redox conditions along chemical pathways between riparian soils
125 and stream sediments are also strongly affected by beaver impoundment. For example, in some
126 systems oxic soils move/regress farther away from the original channel as the water level rises,
127 and the magnitude of anoxic soil area grows accordingly (Naiman et al., 1988). Anoxic
128 conditions can readily develop on the floodplain due to the tranquil flow regime of beaver ponds
129 and large supply of local organic carbon, and along biogeochemically reactive subsurface
130 flowpaths that route floodplain water back to the channel, creating ‘natural reduced zones’
131 (NRZs, e.g. Dwivedi et al., 2018). Anoxic soils may increase the acid neutralizing capacity of the
132 soil water due to the retention of nitrate and sulfate, and act as a net source of iron and
133 ammonium ions (Cirimo and Driscoll, 1993), though quantitative research regarding beaver-
134 induced mobilization of reduced chemical species is generally lacking. Microbial activity of
135 floodplains and riparian zones has been found to be greatly increased by impoundments, a
136 process that has important implications from the pore- to the landscape-scale (Wegener et al.,
137 2017). Enhanced biogeochemical reactivity and potential mobilization of floodplain nutrients,
138 metals, and contaminants necessitates a more complete understanding as beavers are increasingly
139 regarded as a stream restoration solution. Recent studies have signaled beaver-related stream
140 restoration practices may be outpacing fundamental science regarding the wide ranging physical
141 and chemical impacts of such projects (Lautz et al., 2018; Pilliod et al., 2018).

142 For river corridor hydrologic exchanges to be influential to water quality, hydrologic
143 exchange flows need to be both chemically reactive and of appreciable volume compared to river
144 discharge so as to alter net channel solute transport dynamics (Wondzell, 2011). While

145 biogeochemically reactive cross-meander bend hyporheic exchange may be prevalent in most
146 alluvial river corridors, a combination of relatively low hydraulic gradient and tight floodplain
147 soils can limit the impact of this exchange on net river chemistry (Pai et al., 2017), particularly at
148 the km-reach scale. In contrast, beaver dams are known to push large volumes of surface water
149 laterally into the floodplain through engineered fill and spill pathways. Here, we characterize the
150 natural metal transformation and transport dynamics of a specific type of river corridor
151 hydrologic exchange flow, termed here: ‘beaver pond return flows.’ Like the more well-known
152 ‘irrigation return flows’ to rivers driven by the application of water to adjacent cropland (Essaid
153 and Caldwell, 2017), beaver pond return flows are enabled by the purposeful redirection of water
154 outside of the channel. Redirected channel water that is not lost to floodplain evapotranspiration
155 returns to the river in a spectrum of surface flows and subsurface seepage zones (Majerova et al.,
156 2015). By using a combination of remote sensing and direct contact measurements, we identify
157 beaver-induced floodplain exchange flowpaths along two two alluvial mountain streams of
158 varied size. Chemical measurements collected across a full-year hydrological cycle (neglecting
159 winter months) at the pond return flows, and at other observed groundwater seepage types,
160 indicate beaver-induced floodplain exchange can be a dominant mechanism of natural metals
161 flux along alluvial river corridors. Further, extensive deposition of solid metal oxides at return
162 flow discharge points likely provides an important source/sink function for a variety of
163 contaminant transport problems. The evidence to support these statements is shown in the
164 following sections.

165 **2. Materials and Methods**

166 A suite of complementary ground- and drone-based heat tracing and remote sensing
167 methodology was used to characterize the hydrogeological template of beaver-induced
168 floodplain exchange for two alluvial mountain streams of disparate size. A flowpath-oriented
169 perspective to water quality sampling allowed characterization of the chemical evolution of
170 channel water diverted through floodplain ponds and ultimately returned to the channel.

171 *2.1 Study Area*

172 The Lawrence Berkeley National Laboratory Watershed Function Scientific Focus Area
173 (SFA) has established an experimental watershed encompassing the drainages of the East River
174 near Crested Butte, Colorado (USA) to quantify the myriad nested processes impacting the
175 ability of mountainous systems to retain and release water, nutrients, carbon, and metals. This
176 scientific ‘community watershed’ hosts ongoing research spanning a wide range of spatial scales
177 and physical, chemical, and biological processes. The SFA encompasses the drainages of the
178 East River, Washington Gulch, Slate River (including Oh-Be-Joyful Creek), and Coal Creek
179 (Figure 1a). Although each watershed has analogous sections of meandering alluvial stream, they
180 also display unique flow dynamics, current land use practices, and legacies of mining-related
181 contamination. While there is some direct impact from cattle ranching along the East River
182 corridor, that system is generally considered a ‘pristine’ end-member due to the lack of
183 substantial mining activity and ore-rich rock draining its environs. In contrast, Coal Creek and
184 the Slate River are more highly influenced by heavy metals, such as arsenic, copper, cadmium,
185 and zinc due to legacy mine activities in those drainages. For the focus areas of the current study,
186 we chose analogous, meandering open valley sections of the larger East River and smaller Coal
187 Creek with observed contemporary beaver inhabitation (Figure 1a). This research began as

188 broader investigation of natural metal mobility and metal oxide deposition at geologically-
189 controlled groundwater seepages throughout the SFA; however, early in the study, it became
190 apparent that beaver pond return flows were likely to be an important metals flux pathway to
191 consider, and the research plan was adapted accordingly.

192 *2.2 Aerial mapping of floodplain beaver ponds*

193 Floodplain zones inundated with beaver-induced exchange of channel water are difficult
194 to navigate on the ground, but the typical open canopy nature of such areas presents opportunity
195 for small unoccupied aerial vehicle (sUAS, or ‘drone’) and satellite-based mapping techniques.
196 We deployed various multirotor sUAS (3D Robotics Solo, 3D Robotics, Berkeley, CA) at the
197 East River reach from August 12-17, 2017 and July 28-August 2, 2018; and at Coal Creek on
198 July, 31 2018. During sequential flights the sUAS were equipped with various sensors, similar to
199 the approach described by Briggs et al., (2018). For high-resolution visible imagery we used a
200 Ricoh GR11 Camera (Ricoh Imaging Company, Ltd., Japan). Image stills from multiple flight
201 lines, altitudes (generally 200-350 ft above ground surface), and directions were compiled into
202 larger “stitched,” georectified orthoimages of the river corridor using Agisoft PhotoScan
203 software. Position of the aircraft was tracked by internal GPS, and although ground control
204 points were deployed for some flights, they were not used in postprocessing of the visible
205 imagery. Structure from motion (SfM) techniques were then applied using Agisoft PhotoScan
206 software to generate time-specific surface digital elevation models of floodplain structure and
207 exposed channel geomorphology. Details regarding the UAS sensor specifications and the
208 calculated spatial precision of the compiled orthoimages are listed in the public data release of
209 this data at Briggs et al., (2019b). Although the imagery from satellites is of substantially lower
210 resolution than that achievable with sUAS, there may be an existing wealth of historical imagery

211 available to assess longer term beaver pond structure dynamics. We used Google Earth (Google,
212 Mountain View, CA, USA) to qualitatively assess beaver occupation of the Coal Creek reach
213 back to 1999 (earliest available clear imagery).

214 *2.3 Geolocation and characterization of seepage zones*

215 Thermal infrared is sensitive to the water surface ‘skin’ temperature (Handcock et al.,
216 2006) and can be used to geolocate river corridor seepage zones and identify surface water flow
217 patterns at times of natural thermal contrast (Dugdale, 2016; Hare et al., 2015). We expected
218 discharge of deeper groundwater to approximate the surface annual mean temperature
219 (approximately 8°C, Constantz, 2008) whereas shallow groundwater discharge and pond return
220 flows should be warmer in summer, providing multiple characteristic targets for infrared
221 imaging. Thermal infrared data were collected on the ground using handheld FLIR i7 and
222 T600bx series cameras (FLIR Systems, Wilsonville, OR) throughout the beaver-impacted
223 reaches and along an additional approximate 6 km of the upper East River and within the nearby
224 Oh-Be-Joyful Creek drainage. The purpose of the larger-scale thermal infrared mapping was to
225 identify a range of dominant non-beaver-impacted groundwater discharge (seepage) zones for
226 geochemical characterization. To augment the ground-based thermal surveys throughout the
227 beaver-impacted floodplain areas we collected radiometric thermal infrared data from sUAS
228 using a gimbal-mounted FLIR VUE Pro R 13mm camera.

229 Because thermal infrared imaging may not reliably locate submerged seepage zones,
230 particularly in fast flowing rivers (Hare et al., 2015), armored fiber-optic distributed temperature
231 sensing (FO-DTS) cables were deployed along an approximate 2.4 km floodplain channel length
232 at the East River from August 15 to August 22, 2017. FO-DTS technology for environmental
233 temperature sensing is thoroughly reviewed by Tyler et al., (2009). Effort was made to emplace
11

234 the weighted cables along the sediment-water interface of the ‘cutting’ banks of meander bends
235 as these locations typically show enhanced exchange of surface and groundwater. FO-DTS data
236 were collected with a Sensonet Oryx control unit (Sensonet Ltd., United Kingdom) run in
237 double-ended mode at 10-min acquisition time per channel (20-min per measurement) and 1.01
238 m linear spatial resolution.

239 Once seepage zones of various type were identified, stream flow was physically gauged
240 for several of the higher volume discharges using small custom surface weirs, graduated
241 cylinders, and a stopwatch. Slow flowing ‘diffuse’ seepage rates were evaluated at 4 discrete
242 locations along an East River side channel margin, down gradient of a large beaver pond, where
243 seepage was indicated by thermal imaging and Fe-oxide staining from August 23 to November 4,
244 2017. For comparison, seepage was also monitored over this period within an adjacent spatially
245 focused, higher flow beaver pond return seepage zone. Vertical seepage rates were tracked over
246 time using profiles of shallow (0.01, 0.07, 0.11 m depth below sediment-water interface)
247 saturated sediment temperatures collected with iButton thermal data loggers (Maxim Integrated
248 DS1922L) run at 0.0625 °C precision embedded in short steel pipes, as described in detail by
249 Briggs et al. (2014). The workflow suggested by Irvine et al., (2017) that combines diurnal
250 temperature signal-based thermal parameter measurements with diurnal signal amplitude
251 attenuation was used to perform the analytical modeling of vertical water flux rates. The
252 fundamental (diurnal) sinusoids were derived from the raw temperature data using the Captain
253 Toolbox (Young et al., 2010) and VFLUX2 (Irvine et al., 2015) Matlab-based programs. Vertical
254 flux was evaluated over time with the amplitude ratio-based analytical models of VFLUX2, a
255 site-specific thermal diffusivity estimated from vertical diurnal temperature signal transport (e.g.
256 Luce et al., 2013), and an estimated sediment porosity of 0.5 (fine floodplain sediments).

257 *2.4 Water quality monitoring and sampling*

258 Two types of water chemistry data were collected: 1. spatially-distributed synoptics
259 covering seepage zones, off-channel ponded areas, and main channel locations, and 2. main
260 channel high-resolution time series over years 2017-18. Synoptic water samples were collected
261 using 60 mL plastic Luer-Lok syringes and filtered through single-use Millex 0.45- μm Luer-Lok
262 filters. There were four synoptic sampling events in total: 1. August 19-22, 2017; 2. June 21-22,
263 2018; 3. July 29-August 3, 2018; and 4. September 23-25, 2018, with the largest suite of samples
264 collected during event 3, and a subset of sample locations visited during other events. Sample
265 water was stored in 125 or 250 mL polypropylene bottles, preserved with 2-ml trace metal grade
266 HNO_3 , and kept in an ice cooler or refrigerated until evaluated for dissolved Fe, Mn, As, and Al
267 by either the U.S. Geological Survey Water Quality Laboratory or the University of Connecticut
268 Center for Environmental Sciences & Engineering Laboratory. Main channel chemical time
269 series of Fe, Mn, and Al were collected by grab sample every few days from spring into the fall
270 of 2017 and 2018. Time series sample collection locations were approximately 1 km downstream
271 of the Coal Creek and East River beaver-impacted floodplain zones. Stream water samples were
272 collected daily to weekly depending upon snow and ice conditions using an automatic water
273 sampler (Model 3700; Teledyne ISCO, NE, USA), with samples pumped via peristaltic pump
274 into uncapped 1 L polyethylene bottles. Sample bottles were retrieved at regular intervals, with
275 25 mL aliquots filtered (Pall, NY, USA; PTFE; 0.45 μm) and preserved with trace metal grade
276 12 N HNO_3 until analysis. Cation and trace metal concentrations were determined using ion
277 coupled plasma mass spectrometry (ICP-MS) (Element 2, Thermo Fisher, MA, USA).

278 Field parameters (dissolved oxygen (DO), specific conductivity at 25 °C (SpC), and
279 temperature) were typically evaluated at the time of synoptic water sample collection with a

280 SmarTroll MP handheld sensor (In-Situ Inc., United States). DO was also tracked over time in
281 summer 2018 in two of the larger East River floodplain ponds using MiniDOT loggers (Precision
282 Measurement Engineering, Inc., Vista, CA, USA) paired with electrical conductivity/pressure
283 loggers (Solinst Levelogger Junior Edge, Solinst Canada Ltd, Ontario, CAN). To investigate
284 temporal redox dynamics of beaver return flow seepage, a vertical profile of redox potential (Eh)
285 was also collected (surface pool, 0.05, 0.1, 0.15, 0.2, 0.25 m depths) at the same focused return
286 flow seep mentioned above from June 22 to July 13, 2018 using a custom designed logging (1
287 min increments) redox probe (Paleo Terra, Netherlands).

288 Although thermal infrared is useful for locating surface seepage locations, the geometry
289 of the flowpaths that feed those seepage zones, and their connection to upgradient water sources,
290 is typically inferred. However, near-surface electrical geophysical methods can be used to map
291 flowpaths of reduced groundwater, as various redox processes release ions into solution
292 increasing the bulk electrical conductivity (EC) of the subsurface (Binley et al., 2015). We used a
293 hand carried electromagnetic induction GEM-2 frequency-domain instrument (Geophex, Ltd.) to
294 evaluate bulk conductivity of the near surface. Data were collected in the vicinity the East River
295 return flow seeps instrumented with iButton sensors on September 23, 2018 and throughout the
296 Coal Creek beaver-inhabited floodplain corridor on September 25, 2018. The GEM2 tool was
297 operated over 7 frequencies ranging 1,530-93,090 Hz and the expected depth of investigation
298 limit was approximately 5 m. Similar to the groundwater/surface water exchange study of Ong et
299 al. (2010) we did not invert the data but instead work with apparent bulk electrical conductivity
300 (EC) , which was estimated from raw (e.g. not smoothed) quadrature data using EMInvertor
301 software (Geophex, Ltd.) based on the GEM-2 instrument coil separation (1.66 m).

302 **3. Results and Discussion**

303 A combination of drone-based imaging and ground-based heat tracing, geochemical and
304 geophysical measurements indicated beaver-induced floodplain exchanges create important, and
305 perhaps dominant, transport pathways of natural metals. All data presented below are publicly
306 available from Briggs et al., (2019b, 2019a) and Williams et al., (2019).

307 *3.1 Spatial dynamics of geologic seeps and beaver pond return flows*

308 Numerous types of beaver dams, ponds, and return flows were observed along the East
309 River and Coal Creek study reaches, some of which are shown Figure 1b-e. Heat tracing was
310 used to identify spatially preferential channel/floodplain and groundwater connectivity via
311 thermal infrared and FO-DTS technology. Specifically, riverbed interface temperature was
312 recorded with FO-DTS over 6 days in August 2017 along the main East River channel adjacent
313 to the ponded floodplain. Mean temperature along the cables generally ranged from 10.0 to 10.6
314 °C (full diel range of approximately 8 °C or less), showing subtle warming with downstream
315 distance over the 2.5 km beaver impacted reach (Figure 2). No strong cold anomalies
316 approximating deeper groundwater (approximately 7-9 °C) temperature were observed,
317 indicating discharge of deeper flowpaths to the river is likely not an important process of
318 hydrologic exchange along beaver-impacted section of floodplain. This finding is consistent with
319 the FO-DTS-based hydrogeological characterization of Pai et al. (2017) for a meandering reach
320 immediately downstream of our study reach. Although there are several steep, 10's of m high
321 cutbanks into the shale bedrock along the reach that might be expected to produce groundwater
322 seepage (Winter et al., 1998), shale is typically of low permeability and no substantial
323 groundwater discharge was observed from the outcrops over two summer field seasons. A few

324 discrete valley wall seepages were located visually/with infrared, and groundwater discharge
325 from these was captured by beaver ponds before entering the river, as discussed below.

326 Several discrete warm temperature sections are notable in the mean FO-DTS record
327 (Figure 2). During retrieval of the FO-DTS cable, we found that approximately 6 of these warm
328 anomalies resulted from new beaver dam shunts that had been built since the cable was
329 deployed, of the type depicted in Figure 1b. These locations are also indicated by large
330 temperature standard deviation anomalies, as the cable was exposed in part to dynamic air daily
331 temperatures. These high variance zones are spatially coupled with slightly cool, less variant
332 temperatures where the cable was buried inside the dam materials (Figure 2). The fortuitous real
333 time observations of shunt dam building shows channel water diverting structures can be built by
334 beaver in just a few days, altering river/floodplain connectivity in a substantial and sustained
335 way. Two additional discrete sections of FO-DTS cable showed paired warm mean temperatures
336 and low standard deviation ('R' in Figure 2). These are interpreted (and field confirmed with bed
337 temperature probing) as return flow seepage zones, as strong upwelling of even relatively warm
338 water is expected to buffer riverbed interface temperature. Both return flow seepage locations
339 were located adjacent to major floodplain beaver impoundments. Our FO-DTS results show that
340 return flow seepages can be of high enough magnitude to measurably alter sediment-water
341 interface temperature in the main channel of larger, fast flowing rivers where heat tracing
342 methods are typically challenged to locate zones of exchange.

343 Thermal infrared surveys conducted throughout the East River beaver reach in summer
344 2017 and 2018 showed that the floodplain ponds were typically warmer than the main channel
345 by afternoon, and that beaver pond return flows can be identified as warm anomalies (e.g. Figure
346 3C), as indicated by FO-DTS. In contrast one small beaver pond along the steep valley wall of
16

347 Coal Creek was entirely sourced by a large hillslope spring of presumably deeper groundwater
348 (Figure 1d). This spring water was colder than the main channel (Figure 3d), demonstrating that
349 not all return flows will contribute to warming of channel water in summer, which agrees with
350 the finding of Weber et al., (2017) that beavers can enhance thermal heterogeneity (cold and
351 warm) in some systems. However, the larger ponded areas along Coal Creek floodplain away
352 from the valley wall contained relatively warm, diverted channel water, similar to the East River
353 floodplain. A more spatially extensive thermal infrared survey conducted along the upper East
354 River corridor where the valley is much narrower and steeper, and along the bedrock lined, steep
355 Oh-be-Joyful Creek, identified dozens of cold groundwater discharges emanating directly from
356 fractured bedrock. A subset of these ‘geologic’ seeps were sampled for chemical comparison to
357 the beaver pond return flows, as described in Section 3.2 below.

358 Visual imagery collected by sUAS was integrated to build high resolution orthomosaics
359 of the East River (Figure 4) and Coal Creek (Figure 5) beaver reaches. Surface digital elevation
360 models were also derived from the visual imagery and used to infer floodplain surface flow
361 patterns based on elevation changes (Supplemental Figures A1, A2). Although not attempted for
362 this study, such structure-from-motion drone imaging products are likely to be useful for ‘fill and
363 spill’ numerical flow modeling of ponded areas. The 2017 East River orthomosaic demonstrates
364 the extensive saturated floodplain area induced by beaver-induced shunting of channel water
365 (Figure 4a, b). It appeared that just 2 shunts placed at strategic locations, namely at the
366 confluence of a river oxbow and along a river side channel, were responsible for the majority of
367 diverted channel water over both summer seasons (Figure 4 a). These shunts were less effective
368 in July/August 2018 due to a lower flow condition causing widespread draining of the floodplain
369 ponded areas (Figure 4c), though the floodplain morphology appeared comparable to 2017. A

370 rain event the day before the 2017 sUAS mapping mobilized fine sediments and the resulting
371 turbidity was used as a natural qualitative tracer of advective flow connectivity through the
372 linked ponded systems (Figure 4b). These flow patterns indicate preferential pathways through
373 more stagnant ponded areas.

374 The pond systems generally terminated near a large meander bend of the river, where
375 clusters of beaver pond return seeps transferred water back to the channel (Figure 4b, c). No
376 prominent surface return flows were noted in summer 2017 or 2018 along the East River
377 floodplain section. However, a survey in later September 2018 showed that at the lowest channel
378 flow condition beaver were able to build several spanning dams across the East River, diverting
379 more water into the floodplain, refilling and overflowing the ponded areas and creating
380 numerous overland return flows. It may be that alluvial mountain rivers of similar large size to
381 the East River go through a natural beaver diversion cycle: 1. Large spring snow melt pulses
382 damage or destroy the previous year's dam structures (also shown by Briggs et al., (2013)); 2. In
383 early summer river discharge recedes but river stage is still relatively high and shunts are
384 effective to divert water to the floodplain, but channel-spanning dams cannot yet be constructed
385 (Figure 1b); 3. In mid-summer, channel flow drops farther (typically by a factor of 10x from
386 spring peak at the East River, i.e. USGS gage 09112500) and the shunts are less-effective but
387 channel spanning dams cannot yet be built, causing a recession of floodplain pond levels (Figure
388 4c); 4. At the lowest flows in early fall, spanning dams are built, refilling the ponded areas before
389 winter. Longer term, higher-frequency monitoring is needed to explore these temporal dynamics.

390 In contrast to the East River, channel spanning dams were observed along the Coal Creek
391 system across 2017 and 2018 summer and early fall seasons (Figure 5a). Remarkably, each of
392 four successive dams temporarily diverted almost the entirety of channel flow into the adjacent

393 floodplain in 2018 (Figure 5a, c, d), and this diverted water returned to the downstream channel
394 in a series of surface and subsurface return flows. Discharge from two of the larger surface return
395 flows was measured at 173 and 346 m³/d (with mobile weirs) in August 2018, representing a
396 large input of sub-oxic water back to the main channel. Extensive Fe-oxide staining was visible
397 along the floodplain ponded areas (rust colors, Figure 5c), but oxide deposition was not
398 associated with the smaller groundwater spring-fed beaver pond. A downstream ponded
399 floodplain area captured another groundwater discharge originating from a road culvert on the
400 hillslope above the floodplain (Figure 5d), and this oxic groundwater mixed with reduced
401 floodplain water before entering the channel in a series of subsurface seepages. Beaver dam
402 capture of discrete hillslope groundwater discharge was also noted at multiple locations along the
403 East River, indicating that floodplain ponds should be considered in groundwater/surface water
404 exchange studies that are typically focused on hyporheic exchange alone. Google Earth imagery
405 from 1999, 2005, and 2012 of the Coal Creek reach showed similar (to 2018) floodplain pond
406 morphology and the existence of channel spanning dams diverting large portions of streamflow
407 (Supplemental Figure A3), indicating ‘disturbance’ caused by beaver inhabitation may create a
408 relatively stable new floodplain exchange dynamic.

409 *3.2 Dissolved chemistry of beaver-induced floodplain exchanges and geologic seeps*

410 Earlier work has indicated the potential for beaver impoundments to expand zones of
411 reducing conditions in saturated soils (Cirimo and Driscoll, 1993; Naiman et al., 1988). Recently,
412 NRZs have been identified in other Colorado floodplain systems as key locations of nutrient
413 transformation (Boye et al., 2017; Dwivedi et al., 2018) and contaminant accumulation (Janot et
414 al., 2016). However, although NRZs have strong, spatially compressed redox gradients, they are
415 not all likely to function as hotspots of reaction influential to the larger floodplain system

416 chemistry, or ecosystem ‘control points.’ Reducing conditions can develop locally due to
417 enhanced organic carbon availability and/or residence time (Boano et al., 2010), but spatially-
418 compressed redox gradient alone does not indicate mass flux of reduced chemical species. To
419 influence mixed river water metals concentrations, NRZs must also have appreciable advective
420 exchange with the channel. Our sUAS-based surface mapping and return flow observations
421 indicate beaver-induced flowpaths may dominate river-floodplain advective flux compared to
422 other types of lateral exchange in these systems (Figure 7a), but a more quantitative picture is
423 developed with chemical analysis.

424 Synoptic chemical samples were collected at a combination of main channel (29
425 samples), beaver pond (14 samples), beaver pond return flow (17 samples), and geologic seep
426 (14 samples) locations; although all parameters (DO, SpC, Mn, Fe, Al, As) were not always
427 evaluated for each sample. Although floodplain ponds were relatively easy to physically access,
428 sample filters clogged quickly there, practically limiting pond sample numbers. Spot
429 measurements at the time of water sample collection showed return flows had the lowest median
430 DO concentration at 47% saturation (Figure 6a). However, overall return flows ranged from fully
431 anoxic to fully saturated in DO. This large range can be explained by return flows being
432 comprised of both surface and subsurface flowpaths, with the latter generally of considerably
433 lower DO saturation. Surprisingly, most pond samples were super-saturated in DO, owing to
434 abundant observed primary production (filamentous algae) in the shallow open pools, as all
435 samples were taken during daytime hours. The temporal records from the two major East River
436 floodplain beaver ponds show a more complete story, with large swings from daytime DO super
437 saturation (e.g. >11 mg/L DO diurnal swings) to nearly anoxic conditions overnight, suggesting
438 a system with strong continual aerobic respiration (Figure 7b). Elevation-corrected DO saturation

439 was estimated with the Benson and Krause Equations (US Geological Survey, 2011). Oxygen is
440 the master variable that controls redox condition (Zarnetske et al., 2012), so strong daytime
441 photosynthesis signal of beaver ponds can impart a highly dynamic redox signal onto return
442 flowpaths that are otherwise suboxic. The DO time series data indicate that our daytime pond
443 grab samples for dissolved metals may underestimate daily average levels, as night time suboxic
444 conditions would be expected to enhance metal concentrations. As the 2018 summer progressed,
445 the pond became suboxic though extensive pond algae was still observed (Figure 7b), so it is
446 possible net aerobic respiration increased during this period, and/or advective circulation of the
447 ponds decreased at lower water levels.

448 The SpC of beaver pond return flows showed the largest median conductivity at 351.0
449 $\mu\text{S}/\text{cm}$, with the high end of that range driven by seepages (Figure 6b). This result indicated the
450 potential for subsurface return flow pathways to be mapped with electromagnetic imaging due to
451 enhanced bulk EC, as described below. Ponds showed the largest total range as SpC driven in
452 part by pre-sampling precipitation events and mixing with valley wall groundwater discharges.
453 Other types of measured groundwater discharge, predominantly from fractured bedrock, also
454 showed a large range in SpC but the lowest median value at 158.8 $\mu\text{S}/\text{cm}$.

455 Beaver-induced flows were most distinct from other river corridor water sample types in
456 respect to dissolved concentrations of Fe and Mn (Figure 6 c,d; Figure 7c). Return flows
457 averaged (median) 1120.0 and 210.6 $\mu\text{g}/\text{L}$ for Fe and Mn, respectively, with the maximum Fe
458 value of 14,260.0 $\mu\text{g}/\text{L}$ collected in August 2017 at the major East River return flow seepage
459 instrumented with a redox profiler. For contrast, the median Fe and Mn concentrations ($\mu\text{g}/\text{L}$) in
460 the other three types of samples are: channel (169.1 Fe / 4.7 Mn), beaver ponds (366.8 Fe / 19.2
461 Mn) and geologically controlled groundwater (54.9 Fe / 1.3 Mn). As floodplain beaver pond
21

462 water is dominated by channel diversions, with some discrete hillslope groundwater inflow,
463 metal concentrations are clearly increased by beaver-induced hydrologic exchanges.

464 While it is not uncommon to find high concentrations of natural metals in reduced
465 floodplain soil porewater (Schulz-Zunkel and Krueger, 2009), what makes beaver pond return
466 flows unique is that they also show strong advective flux. Hyporheic exchanges in larger river
467 systems often may not substantially impact mixed river solute transport, particularly at the reach-
468 scale (Wondzell, 2011). However, in the East River system dissolved Mn concentrations
469 collected in 4 surveys over a year always increased in mixed main channel water along the
470 beaver-impacted floodplain (Figure 4a). Background concentrations of Mn were substantially
471 higher in the mine-impacted Coal Creek reach, and although channel sampling was more limited,
472 large increases in concentration were observed over just a few hundred meters in the zone of
473 return flows (Figure 5a). Plotting Fe vs Mn for all samples clearly demonstrates how return flows
474 from beaver ponds dominate the anomalously high concentrations observed for both species, and
475 although the ratio of the metals differed, Fe concentrations were almost always dominant (Figure
476 7c) consistent with Fe being preferentially elevated in comparison to Mn in the vast bulk of
477 geologic materials. The mobility of As and Al was enhanced by beaver-induced floodplain
478 exchanges (Figure 6e, f), as discussed in Section 3.3.

479 The spot DO measurements at East River beaver pond return flow seepages all showed
480 varied degrees of suboxic condition (Figure 6a, Briggs et al., 2019a), though temporal redox
481 fluctuations are not clear in these sparse sampling events. However, the redox potential profile
482 collected directly within the return flow seep (shown flowing in Figure 3d) had systematic Eh
483 shifts at all depths at daily to weekly timescales (Figure 7d). Overall there was a transition
484 toward strong reducing conditions from June 22 to July 11, 2018, except in the surface seepage
22

485 pool where the probe was likely exposed to air periodically. The reducing shift likely results
486 from the observed decreased seepage rates over time. Total flow from the seepage was
487 physically measured to be 1464 L/d in late June but was too low to be reliably captured with the
488 surface weir in late July, a reduction explained by the observed recession of the upgradient pond
489 level during this period (decreased lateral hydraulic gradient). Vertical seepage rates measured
490 over 70 d in 2017 using iButton temperature sensors installed in this seep show coordinated short
491 (daily) and longer-term flux patterns, also indicating that seepage redox chemistry (and
492 associated metal concentrations) is likely to fluctuate over time (Figure 7a). As discussed in
493 detail by Briggs et al. (2013), reactive mass flux beaver pond return seepages are not likely to
494 occur at highest metal concentration but when fluid flux and concentration (typically inversely
495 related) are optimally balanced. Therefore, higher flux surface return flows of lower metal
496 concentration may be more important to river chemical dynamics than strongly reduced focused
497 seepages. For example, the predominant East River return flow seepage transferred
498 approximately 10 g/d of dissolved Fe²⁺ to the main channel at times during this study, while the
499 larger Coal Creek surface return flow transferred approximately 218 g/d Fe²⁺.

500 In general, the focused return seepage water was less reduced toward the land surface
501 along the redox profiler, indicating some vertical diffusive exchange with surface oxygen, and/or
502 a convergence with oxic subsurface flowpaths at the seepage zone. During redox probe
503 installation it was clear that beneath approximately 10 cm of fine sediments the focused seepage
504 zone sediments were composed of higher permeability sands and gravels. As has been observed
505 for numerous other river corridor seepage types, the distribution of spatially focused return flow
506 seepages is likely controlled by existing heterogeneous floodplain geologic deposits where
507 relatively coarse alluvium creates conduits of hydrologic exchange.

508 The areal ‘footprint’ of sub-oxic return flowpaths was mapped from the land surface
509 using electromagnetic imaging. Higher frequencies of the GEM2 tool should represent more
510 shallow subsurface bulk EC dynamics, so raw data from the highest four frequencies (of 7 total
511 frequencies) were arithmetically averaged for this analysis, as the lowest 3 frequencies were
512 found to have reduced sensitivity in these systems. The resulting map of electrically-conductive
513 subsurface anomalies below a larger beaver pond at the East River indicated a swath of reduced
514 water 10’s of meters across flowing in the shallow subsurface toward the river, some of which
515 discharges at the focused seep where the redox probe was installed (Figure 4c). These reactive
516 flowpaths also source the diffuse seepage zones along the main channel margin, including the
517 Fe-rich side channel shown in Figures 1d) and e). In general, electromagnetic imaging data
518 collected throughout the channel area and over the opposite bank floodplain where there was no
519 beaver activity did not indicate extensive subsurface plumes of metal-impacted water (Figure
520 4c). Vertical seepage rates along the channel margin were slow, typically less than 0.2 m d^{-1} over
521 the 2017 period monitored with vertical iButtons (Figure 7a), but spatially extensive enough to
522 drive the DO content of the side channel surface water down to an average of 54% saturation in
523 mid-day during the summer 2018. Vertical seepage rates during the same period in 2017 for the
524 focused beaver return flow seepage zone were stronger, ranging up to 0.6 m/d . Diffuse seepage
525 rates at all 4 locations showed coordinated short-term shifts to downward flow, likely due to
526 higher event flows in the channel. In contrast, discharge from the focused bank seep showed a
527 different temporal pattern that is likely driven by beaver pond stage dynamics, and not directly
528 impacted by channel flow.

529 A larger area was imaged along the Coal Creek, revealing 3 major ‘hot spots’ of
530 increased shallow bulk EC (Figure 4b). The two upstream zones are adjacent to the main

531 floodplain ponded areas in the vicinity of observed return flow seepages. This result agrees with
532 the East River imaging, in that although seepages may be highly focused in space at the land
533 surface, they are fed and underlain by larger subsurface plumes of reduced metals. Of note, the
534 downstream surface return flows, although enriched in Fe and Mn compared to channel water, do
535 not create any extensive electromagnetic anomaly. This may be surprising given the extensive
536 visible Fe staining along the creek sediments in this area (Figure 5c), but the GEM2 tool is
537 sensitive to the upper several meters of earth material, and therefore this result indicates that the
538 surficial return flows are not underlain by extensive subsurface reduced plumes. Much of the Fe
539 oxides visible in this area may be precipitating from the nearby upstream highly reduced return
540 flow subsurface seepages, and/or from the moderate concentrations of reduced Fe measured in
541 the surface return flows. Further downstream, a channel spanning dam diverts channel water to
542 both the right and left bank floodplain areas (Figure 5d). Flowpaths along the right bank
543 appeared to stay on the land surface, remained oxic, and there was little enhancement of
544 subsurface bulk EC. However, the downstream left floodplain area was highly reduced, mixing a
545 valley wall groundwater seep with diverted channel water that returned to the stream in a series
546 of seepages. Fe staining was prevalent in this area, and the floodplain pools and shallow
547 subsurface highly electrically conductive (Figure 5b).

548 The main channel chemical time series (Fe, Mn, Al) were collected approximately 1 km
549 downstream of each beaver-impacted reach (Figure 8). In total 299 samples were collected at the
550 East River and 340 samples collected at Coal Creek over the 2017/2018 period. Main channel Fe
551 concentrations were typically measurable, indicating persistent inflow from reduced seepages.
552 There was a bimodal pattern with early and late season peaks in concentration (over 50 ppb) at
553 the East River that may be tied to the strong early and late season beaver-induced floodplain

554 connection mentioned above (Figure 8a). Mn was generally quite low or below the detection
555 limit, except for a few spikes coinciding with Fe highs. When East River Fe and Al are plotted
556 against each other there is no strong proportional relation (Figure 8b), indicating other processes
557 in addition to reduced return flows drive Al concentration dynamics. This may be explained in
558 part by the high concentrations of Al observed at the floodplain valley wall geologic
559 groundwater seepages, such that some combination of groundwater discharge and beaver-
560 induced floodplain exchange influences downstream Al concentration. A bimodal temporal
561 pattern of main channel Fe concentration was also observed at Coal Creek (Figure 8c), where Mn
562 concentrations were generally much higher than at East River and better coupled with Fe. A
563 strong proportional relation was observed between Fe and Al at Coal Creek indicating that for
564 that system reduced return flow seepages may drive Al mobility (Figure 8d). Unlike the East
565 River, Al concentration in the local Coal Creek beaver-impacted reach hillslope groundwater
566 was low, based on limited data.

567 *3.3 Metal oxide deposition at beaver pond return flows*

568 Oxides and hydroxides (referred to here by the general term “oxides”) of Mn and Fe
569 metals are often associated with groundwater seepage zones (Boano et al., 2014; Gandy et al.,
570 2007) and characteristic red staining of surface sediments is frequently used to visually locate
571 points of sub-oxic seepage (e.g. Figure 1e; Figure 5c,d). Similar to engineered geochemical
572 barriers using zero-valent Fe (McCobb et al., 2018), metal oxides function as a sorption sink for
573 a host of dissolved contaminants toxic to humans and aquatic life. In watersheds, such as Coal
574 Creek that are impacted by mine water drainage, Mn oxides have been shown to sorb and co-
575 precipitate cobalt, nickel, and zinc in high concentrations (Jenne, 1968). Fe oxides have also
576 been shown to substantially reduce these contaminants as groundwater flows through the

577 streambed, and to be a strong sink for arsenic (Nagorski and Moore, 1999). In zones of uranium
578 contamination, adsorption to biogenic Fe oxides can strip hexavalent uranium (U(VI)) from
579 groundwater (Katsoyiannis, 2007) before discharge to surface water. Fe oxides have also been
580 shown as important sorption sites for perfluorooctane sulfonate (PFOS) (Johnson et al., 2007), a
581 contaminant of major emerging concern (Banzhaf et al., 2016). However, dynamic dissolution of
582 oxides under dynamic reducing conditions of beaver-impacted floodplain soils can mobilize
583 previously sequestered contaminants along with the dissolved metals.

584 Along the river corridor, solid grain Fe and Mn is typically found in glacial sediment
585 grains, alluvial sediments, and mine tailings. Reduction to soluble form under suboxic condition
586 mobilizes the metals to travel with hyporheic flow, groundwater, or as this study has shown, in
587 surface return flows and subsurface seepages. Widespread Fe staining below return flow
588 discharge points along the East River and Coal Creek corridors visibly indicates how beaver
589 activity can greatly alter metal oxide dynamics in alluvial systems (Figure 5c, d). For example, a
590 side channel along the East River adjacent to the return seepages that was instrumented with
591 iButtons and the redox probe, was shown to collect reduced water loaded with natural metals
592 (Figure 1e), and precipitate oxides as this water exchanged gas with air and advectively mixed
593 with the main channel.

594 Arsenic and aluminum concentrations were predominantly higher in the mine-impacted
595 Coal Creek return flow samples as compared to the East River, averaging 6.3 and 10.1 $\mu\text{g/L}$,
596 respectively. These concentrations are approximately 2x higher than that observed in the diverted
597 channel water, suggesting the mobility of these contaminants is tied to the dissolution of
598 floodplain metal oxides. Considering the importance of metal oxides to a host of abiotic and
599 biotic processes, beaver pond return flows of reduced water could be recognized as ecosystem
27

600 control points (Bernhardt et al., 2017), and deserve similar research attention to more commonly
601 studied mechanisms of river to floodplain hydrologic exchange. Several western USA alluvial
602 river corridors with similar morphology to East River have contemporary U(VI) contamination
603 concerns resulting from legacy floodplain mine tailings (Curtis et al., 2006; Naftz et al., 2018),
604 and it has been shown that mobility of U(VI) is directly tied to Fe oxide dynamics in NRZs
605 (Bone et al., 2017; Davis et al., 2006). In such systems the return of beaver, or human simulation
606 of their dam construction using dam analogues, may result in undesirable transport of
607 contaminants.

608 **4. Conclusions**

609 Enhanced river/floodplain hydrologic connection has been shown to increase river
610 corridor evapotranspiration and net carbon uptake (Missik et al., 2018), but the impact of beaver-
611 induced floodplain water flux on the mobility of river corridor metals has been largely under-
612 characterized. In the two alluvial systems studied here, we observed high-flow active shunting of
613 stream water onto adjacent floodplains, greatly expanding the volume of saturated floodplain
614 sediments with strong hydrologic connectivity to the channel. Land surface and subsurface
615 beaver pond return flows contained high concentrations of dissolved Mn and Fe, redox-sensitive
616 metals that are highly influential to a multitude of biogeochemical and abiotic processes.
617 Dissolution of solid phase floodplain sediment Mn and Fe oxides can provide an advective
618 pathway for contaminant transport, particularly in mine-impacted watersheds. In contrast to
619 episodic overbank river flow events or slower-exchanging meander bend flowpaths, beaver-
620 induced exchanges can provide strong, persistent river-floodplain connectivity and conduits for
621 metal mobility. As beaver return to alluvial floodplain systems across north America, active

622 human management will likely need to consider system-specific consequences of enhanced
623 exchange with suboxic floodplain waters, to be balanced against numerous desirable
624 hydroecological and restorative outcomes.

625

626 **Acknowledgments**

627 Funding for this methods development was provided by U.S. Department of Energy grant DE-
628 SC0016412 and the U.S. Geological Survey (USGS) Toxic Substances Hydrology Program. This
629 material is partially based upon work supported through the Lawrence Berkeley National
630 Laboratory's Watershed Function Scientific Focus Area. The U.S. Department of Energy (DOE),
631 Office of Science, Office of Biological and Environmental Research, Subsurface
632 Biogeochemical Research Program funded the work under contract DE-AC02-05CH11231
633 (Lawrence Berkeley National Laboratory; operated by the University of California). We thank
634 Jennifer Reithel and the Rocky Mountain Biological Laboratory for logistical support; Lee
635 Slater, Dylan Fosberg, Kimberly Moore, Cian Dawson, Eric White, Josip Adams, Christopher
636 Holmquist-Johnson, Jalise Wright, and Bianca Isabelle Abrera for field data collection;
637 Rosemary Carroll for providing the HUC boundaries used in Figure 1; Mike Wilkins and other
638 anonymous reviewers for peer review early drafts. Any use of trade, firm, or product names is
639 for descriptive purposes only and does not imply endorsement by the U.S. Government.

640

641

642

643

644

645 **References**

- 646 Bailey, D.R., Dittbrenner, B.J., Yocom, K.P., 2019. Reintegrating the North American beaver
647 (Castor canadensis) in the urban landscape. WIREs Water 6.
648 <https://doi.org/10.1002/wat2.1323>
- 649 Banzhaf, S., Sparrenbom, C.J., Banzhaf, S., Filipovic, M., Lewis, J., Sparrenbom, C.J., Barthel,
650 R., 2016. A review of contamination of surface- , ground- , and drinking water in Sweden
651 by perfluoroalkyl and polyfluoroalkyl ... Ambio. <https://doi.org/10.1007/s13280-016-0848-8>
- 652 Boano, F., Demaria, A., Revelli, R., Ridolfi, L., 2010. Biogeochemical zonation due to
653 intrameander hyporheic flow. Water Resour. Res. 46, W02511.
654 <https://doi.org/10.1029/2008wr007583>
- 655 Boano, F., Harvey, J.W., Marion, A., Packman, A.I., Revelli, R., Ridolfi, L., Worman, A., 2014.
656 Hyporheic flow and transport processes: Mechanisms, models, and biogeochemical
657 implications. Rev. Geophys. 1–77. <https://doi.org/10.1002/2012RG000417>.Received
- 658 Bone, S.E., Cahill, M.R., Jones, M.E., Fendorf, S., Davis, J., Williams, K.H., Bargar, J.R., 2017.
659 Oxidative Uranium Release from Anoxic Sediments under Diffusion- Limited Conditions.
660 Environ. Sci. Technol. 51, 11039–11047. <https://doi.org/10.1021/acs.est.7b02241>
- 661 Bouwes, N., Weber, N., Jordan, C.E., Saunders, W.C., Tattam, I.A., Volk, C., Wheaton, J.M.,
662 Pollock, M.M., 2016. Ecosystem experiment reveals benefits of natural and simulated
663 beaver dams to a threatened population of steelhead (*Oncorhynchus mykiss*). Nat. Sci.
664 Reports 1–13. <https://doi.org/10.1038/srep28581>
- 665 Boye, K., Noël, V., Tfaily, M.M., Bone, S.E., Williams, K.H., Bargar, J.R., Fendorf, S., 2017.

666 Thermodynamically controlled preservation of organic carbon in floodplains. *Nat. Geosci.*
667 10, 415–419. <https://doi.org/10.1038/NGEO2940>

668 Briggs, M.A., Chen, W., Slater, L.D., Day-Lewis, F.D., 2019a. Hydrogeochemical data for the
669 characterization of stream, groundwater, and beaver-induced floodplain exchange in the
670 East River Science Focus Area, Crested Butte, CO. U.S. Geol. Surv. Data Release.
671 <https://doi.org/10.5066/P9Q1Z1TK>

672 Briggs, M.A., Dawson, C.B., Holmquist-Johnson, C.L., Williams, K.H., Lane, J.W., 2019.
673 Efficient hydrogeological characterization of remote stream corridors using drones. *Hydrol.*
674 *Process.* 33. <https://doi.org/10.1002/hyp.13332>

675 Briggs, M.A., Dawson, C.B., White, E.A., Holmquist-Johnson, C.L., 2019b. Thermal infrared,
676 multispectral, and photogrammetric data collected by drone for hydrogeologic analysis of
677 the East River and Coal Creek beaver-impacted corridors near Crested Butte, Colorado.
678 U.S. Geol. Surv. Data Release. <https://doi.org/10.5066/P9YWSJ2J>

679 Briggs, M.A., Lautz, L.K., Buckley, S.F., Lane, J.W., 2014. Practical limitations on the use of
680 diurnal temperature signals to quantify groundwater upwelling. *J. Hydrol.* 519, 1739–1751.
681 <https://doi.org/10.1016/j.jhydrol.2014.09.030>

682 Briggs, M.A., Lautz, L.K., Hare, D.K., González-Pinzón, R., 2013. Relating hyporheic fluxes,
683 residence times, and redox-sensitive biogeochemical processes upstream of beaver dams.
684 *Freshw. Sci.* 32, 622–641. <https://doi.org/10.1899/12-110.1>

685 Burchsted, D., Daniels, M., Thorson, R., Vokoun, J., 2010. The River Discontinuum: Applying
686 Beaver Modifications to Baseline Conditions for Restoration of Forested Headwaters.

687 Bioscience 60, 908–922. <https://doi.org/10.1525/bio.2010.60.11.7>

688 Catalán, N., Herrero Ortega, S., Gröntoft, H., Hilmansson, T.G., Bertilsson, S., Wu, P., Levanoni,
689 O., Bishop, K., Bravo, A.G., 2017. Effects of beaver impoundments on dissolved organic
690 matter quality and biodegradability in boreal riverine systems. *Hydrobiologia* 793, 135–148.
691 <https://doi.org/10.1007/s10750-016-2766-y>

692 Cirno, C.P., Driscoll, C.T., 1993. Beaver pond biogeochemistry: Acid neutralizing capacity
693 generation in a headwater wetland. *Wetlands* 13, 277–292.

694 Collen, P., Gibson, R.J., 2000. The general ecology of beavers (*Castor* spp.), as related to their
695 influence on stream ecosystems and riparian habitats, and the subsequent effects on fish - A
696 review. *Rev. Fish Biol. Fish.* 10, 439–461. <https://doi.org/10.1023/A:1012262217012>

697 Constantz, J., 2008. Heat as a tracer to determine streambed water exchanges. *Water Resour.*
698 *Res.* 44, 1–20. <https://doi.org/10.1029/2008WR006996>

699 Covino, T., 2017. Hydrologic connectivity as a framework for understanding biogeochemical
700 flux through watersheds and along fluvial networks. *Geomorphology* 277, 133–144.
701 <https://doi.org/10.1016/j.geomorph.2016.09.030>

702 Curtis, G.P., Davis, J. a., Naftz, D.L., 2006. Simulation of reactive transport of uranium(VI) in
703 groundwater with variable chemical conditions. *Water Resour. Res.* 42, 1–15.
704 <https://doi.org/10.1029/2005WR003979>

705 Davis, J.A., Curtis, G.P., Wilkins, M.J., Kohler, M., Fox, P., Naftz, D.L., Lloyd, J.R., 2006.
706 Processes affecting transport of uranium in a suboxic aquifer. *Phys. Chem. Earth, Parts*
707 *A/B/C* 31, 548–555. <https://doi.org/10.1016/j.pce.2006.04.005>

- 708 Dugdale, S.J., 2016. A practitioner's guide to thermal infrared remote sensing of rivers and
709 streams: recent advances, precautions and considerations. *WIREs Water*.
710 <https://doi.org/10.1002/wat2.1135>
- 711 Dwivedi, D., Arora, B., Steefel, C.I., Dafflon, B., Versteeg, R., 2018. Hot Spots and Hot
712 Moments of Nitrogen in a Riparian Corridor. *Water Resour. Res.* 54, 205–222.
713 <https://doi.org/10.1002/2017WR022346>
- 714 Essaid, H.I., Caldwell, R.R., 2017. Science of the Total Environment Evaluating the impact of
715 irrigation on surface water – groundwater interaction and stream temperature in an
716 agricultural watershed. *Sci. Total Environ.* 599–600, 581–596.
717 <https://doi.org/10.1016/j.scitotenv.2017.04.205>
- 718 Gandy, C.J., Smith, J.W.N., Jarvis, A.P., 2007. Attenuation of mining-derived pollutants in the
719 hyporheic zone : A review. *Sci. Total Environ.* 373, 435–446.
720 <https://doi.org/10.1016/j.scitotenv.2006.11.004>
- 721 Handcock, R.N., Gillespie, a. R., Cherkauer, K. a., Kay, J.E., Burges, S.J., Kampf, S.K., 2006.
722 Accuracy and uncertainty of thermal-infrared remote sensing of stream temperatures at
723 multiple spatial scales. *Remote Sens. Environ.* 100, 427–440.
724 <https://doi.org/10.1016/j.rse.2005.07.007>
- 725 Hare, D.K., Briggs, M.A., Rosenberry, D.O., Boutt, D.F., Lane, J.W., 2015. A comparison of
726 thermal infrared to fiber-optic distributed temperature sensing for evaluation of groundwater
727 discharge to surface water. *J. Hydrol.* 530, 153–166.
728 <https://doi.org/10.1016/j.jhydrol.2015.09.059>

729 Harvey, J.W., Gooseff, M.N., 2015. River corridor science: Hydrologic exchange and ecological
730 consequences from bedforms to basins. *Water Resour. Res.* 51, 1–30.
731 <https://doi.org/10.1002/2015WR017617>.Received

732 Hood, G., 2011. *The Beaver Manifesto*. Rocky Mountain Books, Calgary, CAN.

733 Hood, G.A., Bayley, S.E., 2008. Beaver (*Castor canadensis*) mitigate the effects of climate on
734 the area of open water in boreal wetlands in western Canada. *Biol. Conserv.* 141, 556–567.
735 <https://doi.org/10.1016/j.biocon.2007.12.003>

736 Irvine, D.J., Briggs, M.A., Cartwright, I., Scruggs, C.R., Lautz, L.K., 2017. Improved Vertical
737 Streambed Flux Estimation Using Multiple Diurnal Temperature Methods in Series.
738 *Groundwater* 55. <https://doi.org/10.1111/gwat.12436>

739 Irvine, D.J., Lautz, L.K., Briggs, M.A., Gordon, R.P., Mckenzie, J.M., 2015. Experimental
740 evaluation of the applicability of phase, amplitude, and combined methods to determine
741 water flux and thermal diffusivity from temperature time series using VFLUX 2. *J. Hydrol.*
742 531, 728–737.

743 Janot, N., Lezama Pacheco, J.S., Pham, D.Q., O’Brien, T.M., Hausladen, D., Noël, V., Lallier,
744 F., Maher, K., Fendorf, S., Williams, K.H., Long, P.E., Bargar, J.R., 2016. Physico-
745 Chemical Heterogeneity of Organic-Rich Sediments in the Rifle Aquifer, CO: Impact on
746 Uranium Biogeochemistry. *Environ. Sci. Technol.* 50, 46–53.
747 <https://doi.org/10.1021/acs.est.5b03208>

748 Jenne, E.A., 1968. Chapter 21: Controls on Mn, Fe, Co, Ni, Cu, and Zn concentrations in soils
749 and water: the significant role of hydrous Mn and Fe oxides, in: *Trace Inorganics in Water*.

750 American Chemical Society, pp. 337–387. <https://doi.org/10.1021/ba-1968-0073.ch021>

751 Jin, L., Siegel, D.I., Lautz, L.K., Otz, M.H., 2009. Transient storage and downstream solute
752 transport in nested stream reaches affected by beaver dams. *Hydrol. Process.* 23, 2438–
753 2449. [https://doi.org/Cited By \(since 1996\) 1Export Date 4 April 2012](https://doi.org/Cited%20By%20(since%201996)%201Export%20Date%204%20April%202012)

754 Johnson, R.L., Anschutz, A.J., Smolen, J.M., Simcik, M.F., Penn, R.L., 2007. The Adsorption of
755 Perfluorooctane Sulfonate onto Sand, Clay, and Iron Oxide Surfaces. *J. Chem. Eng. Data*
756 52, 1165–1170. <https://doi.org/10.1021/je060285g>

757 Katsoyiannis, I.A., 2007. Carbonate effects and pH-dependence of uranium sorption onto
758 bacteriogenic iron oxides : Kinetic and equilibrium studies. *J. Hazard. Mater.* 139, 31–37.
759 <https://doi.org/10.1016/j.jhazmat.2006.05.102>

760 Lautz, L., Kelleher, C., Vidon, P., Coffman, J., Riginos, C., Copeland, H., 2018. Restoring
761 stream ecosystem function with beaver dam analogues: Let’s not make the same mistake
762 twice. *Hydrol. Process.* 174–177. <https://doi.org/10.1002/hyp.13333>

763 Ligon, F.K., Dietrich, W.E., Trush, W.J., 1995. Downstream Ecological Effects of Dams.
764 *Bioscience* 45, 183–192. <https://doi.org/10.2307/1312557>

765 Luce, C.H., Tonina, D., Gariglio, F., Applebee, R., 2013. Solutions for the diurnally forced
766 advection-diffusion equation to estimate bulk fluid velocity and diffusivity in streambeds
767 from temperature time series. *Water Resour. Res.* 49, 488–506.
768 <https://doi.org/10.1029/2012WR012380>

769 Majerova, M., Neilson, B.T., Schmadel, N.M., Wheaton, J.M., Snow, C.J., 2015. Impacts of
770 beaver dams on hydrologic and temperature regimes in a mountain stream. *Hydrol. Earth*

771 Syst. Sci. 3541–3556. <https://doi.org/10.5194/hess-19-3541-2015>

772 McCobb, T.D., Briggs, M.A., LeBlanc, D.R., Day-Lewis, F.D., Johnson, C.D., 2018. Evaluating
773 long-term patterns of decreasing groundwater discharge through a lake-bottom permeable
774 reactive barrier. *J. Environ. Manage.* 220, 233–345.
775 <https://doi.org/10.1016/j.jenvman.2018.02.083>

776 Missik, J.E.C., Liu, H., Gao, Z., Huang, M., Chen, X., Arntzen, E., Mcfarland, D.P., Ren, H.,
777 Titzler, P.S., Jonathan, N., 2018. Groundwater - river water exchange enhances growing
778 season evapotranspiration and carbon uptake in a semi - arid riparian ecosystem.
779 <https://doi.org/10.1029/2018JG004666>

780 Naftz, D.L., Fuller, C.C., Runkel, R.L., Briggs, M.A., Solder, J.E., Cain, D.J., Short, T.M.,
781 Gardner, P.M., Byrne, P., Terry, N., Gobel, D., 2018. Hydrologic, biogeochemical, and
782 radon data collected within and adjacent to the Little Wind River near Riverton, Wyoming.
783 US Geol. Surv. Data Release.

784 Nagorski, S.A., Moore, J.N., 1999. Arsenic mobilization in the hyporheic zone of a stream 35,
785 3441–3450.

786 Naiman, R.J., Johnston, C.A., Kelley, J.C., 1988. Alteration of North American Streams by
787 Beaver. *Bioscience* 38, 753–762. <https://doi.org/10.2307/1310784>

788 Naiman, R.J., Melillo, J.M., Hobbie, J.E., 1986. Ecosystem alteration of boreal forest streams by
789 beaver (*Castor canadensis*). *Ecology* 67, 1254–1269.

790 Nash, C.S., Selker, J.S., Grant, G.E., Lewis, S.L., Noël, P., 2018. A physical framework for
791 evaluating net effects of wet meadow restoration on late - summer streamflow.

792 Ecohydrology 1–15. <https://doi.org/10.1002/eco.1953>

793 Pai, H., Malenda, H.F., Briggs, M.A., Singha, K., González-Pinzón, R., Gooseff, M.N., Tyler,
794 S.W., 2017. Potential for Small Unmanned Aircraft Systems Applications for Identifying
795 Groundwater-Surface Water Exchange in a Meandering River Reach. *Geophys. Res. Lett.*
796 44. <https://doi.org/10.1002/2017GL075836>

797 Pilliod, D.S., Rohde, A.T., Charnley, S., Davee, R.R., Dunham, J.B., Gosnell, H., Grant, G.E.,
798 Hausner, M.B., Huntington, J.L., Nash, C., 2018. Survey of Beaver-related Restoration
799 Practices in Rangeland Streams of the Western USA. *Environ. Manage.* 61, 58–68.
800 <https://doi.org/10.1007/s00267-017-0957-6>

801 Poole, G.C., 2010. Stream hydrogeomorphology as a physical science basis for advances in
802 stream ecology. *J. N. Am. Benthol. Soc* 29, 12–25. <https://doi.org/10.1899/08-070.1>

803 Sawyer, A.H., Kaplan, L.A., Lazareva, O., Michael, H.A., 2014. Hydrologic dynamics and
804 geochemical responses within a floodplain aquifer and hyporheic zone during Hurricane
805 Sandy. *Water Resour. Res.* 50, 4877–4892.
806 <https://doi.org/10.1002/2013WR015101>.Received

807 Schulz-Zunkel, C., Krueger, F., 2009. Trace Metal Dynamics in Floodplain Soils of the River
808 Elbe : A Review. *J. Environ. Qual.* 38, 1349–1362. <https://doi.org/10.2134/jeq2008.0299>

809 Seton E.T., 1929. *Lives of Game Animals*. Doubleday, Doran & Co., Garden City N.Y.

810 Tyler, S.W., Selker, J.S., Hausner, M.B., Hatch, C.E., Torgersen, T., Thodal, C.E., Schladow,
811 S.G., 2009. Environmental temperature sensing using Raman spectra DTS fiber-optic
812 methods. *Water Resour. Res.* 45, 1–11. <https://doi.org/10.1029/2008WR007052>

813 US Geological Survey, 2011. Change to solubility equations for oxygen in water: Office of
814 Water Quality Technical Memorandum 2011.03.
815 <https://doi.org//admin/memo/QW/qw11.03.pdf>

816 Vidon, P., Allan, C., Burns, D., Duval, T.P., Gurwick, N., Inamdar, S., Lowrance, R., Okay, J.,
817 Scott, D., Sebestyen, S., Allan, C., Burns, D., Duval, T.P., Gurwick, N., Inamdar, S., Low-,
818 R., 2010. Hot spots and hot moments in riparian zones: potential for improved water quality
819 management. *J. Am. water Resour. Assoc.* 46, 278–298.

820 Weber, N., Bouwes, N., Pollock, M.M., Volk, C., Wheaton, M., Wathen, G., Wirtz, J., Jordan,
821 C.E., 2017. Alteration of stream temperature by natural and artificial beaver dams.
822 *PLoS ONE* 12, 1–23. <https://doi.org/10.17605/OSF.IO/6MMGZ.Funding>

823 Wegener, P., Covino, T.P., Wohl, E.E., 2017. Beaver-mediated lateral hydrologic connectivity,
824 fluvial carbon and nutrient flux, and aquatic ecosystem metabolism. *Water Resour. Res.* 53,
825 4606–4623. <https://doi.org/10.1002/2016WR019538.Received>

826 Westbrook, C.J., Cooper, D.J., Baker, B.W., 2006. Beaver dams and overbank floods influence
827 groundwater-surface water interactions of a Rocky Mountain riparian area. *Water Resour.*
828 *Res.* 42, 1–12. <https://doi.org/10.1029/2005WR004560>

829 Williams, K.H., 2019. Geochemical data from the East River Science Focus Area. DOE public
830 data release.

831 Winter, T.C., Harvey, J.W., Franke, O.L., Alley, W.M., 1998. Ground water and surface water; a
832 single resource. U . S . Geol. Surv. Circ. 1139 79.

833 Wohl, E.E., Lane, S.N., Wilcox, A.C., 2015. The science and practice of river restoration. *Water*

834 Resour. Res. 51, 5974–5997. <https://doi.org/10.1002/2014WR016874>

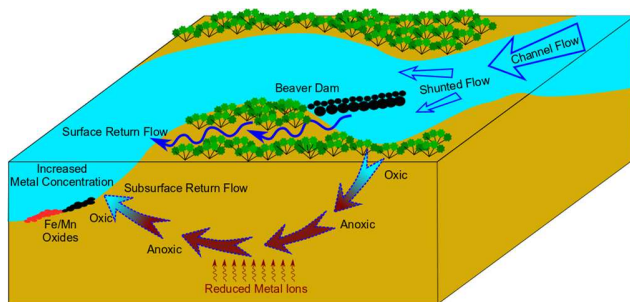
835 Wondzell, S.M., 2011. The role of the hyporheic zone across stream networks. *Hydrol. Process.*
836 25, 3525–3532. <https://doi.org/10.1002/hyp.8119>

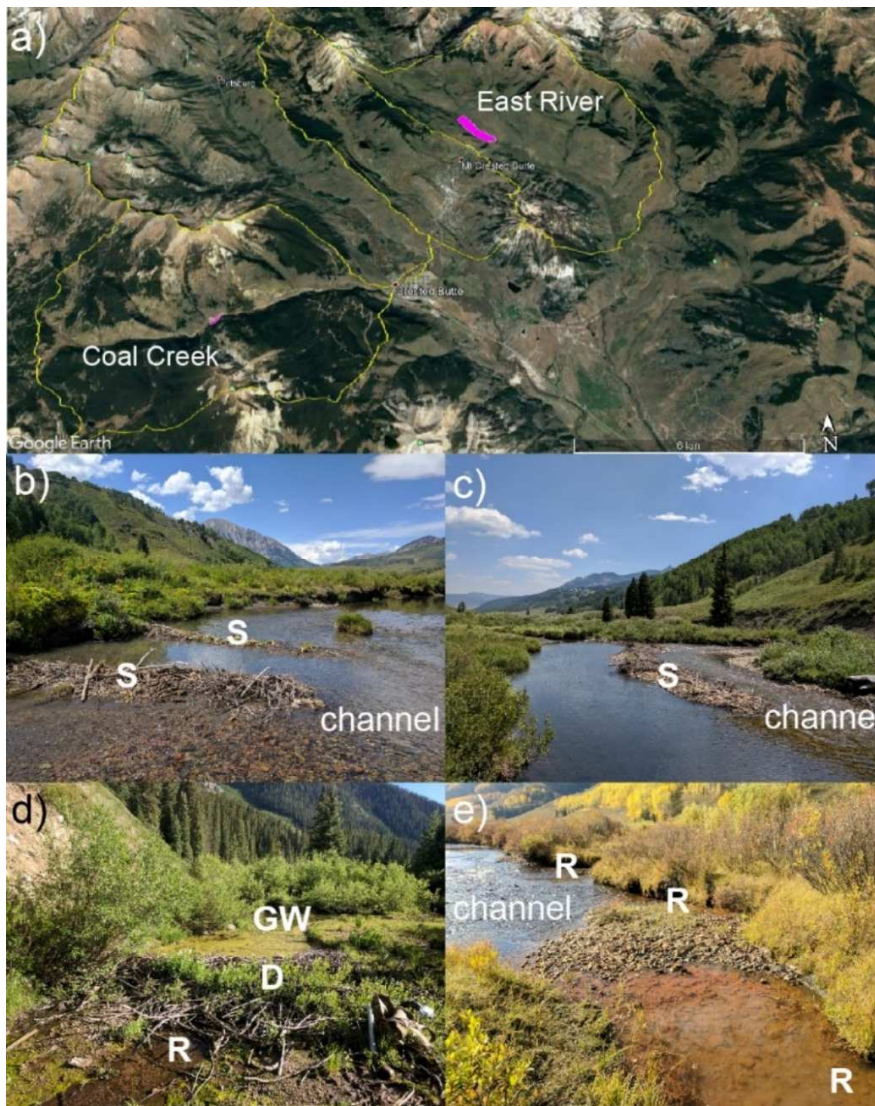
837 Young, P.C., Taylor, C.J., Tych, W., Pegregal, D.J., McKenna, P.G., 2010. *The Captain*
838 *Toolbox*, Centre for Research on Environmental Systems and Statistics, Lancaster
839 University. UK.

840 Zarnetske, J.P., Haggerty, R., Wondzell, S.M., Bokil, V.A., González-Pinzón, R., 2012. Coupled
841 transport and reaction kinetics control the nitrate source-sink function of hyporheic zones.
842 *Water Resour. Res.* 48, W11508. <https://doi.org/10.1029/2012WR011894>

843

844 Graphical Abstract



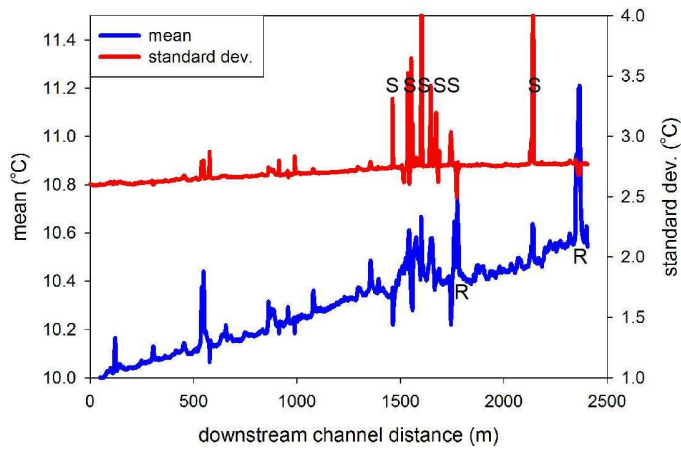


847

848 Figure 1. Panel a) shows the sub-watersheds of the East River SFA, where the Coal Creek and
 849 East River beaver-impacted study floodplain sections are highlighted in pink. In spring and
 850 summer, beavers construct a series of dams at the East River to ‘shunt’ (S) large volumes of
 851 channel water onto the adjacent floodplain (panels b,c). Discrete hillslope groundwater (GW)
 852 springs may be directly captured by small beaver dams (D) (panel d) before draining to the main

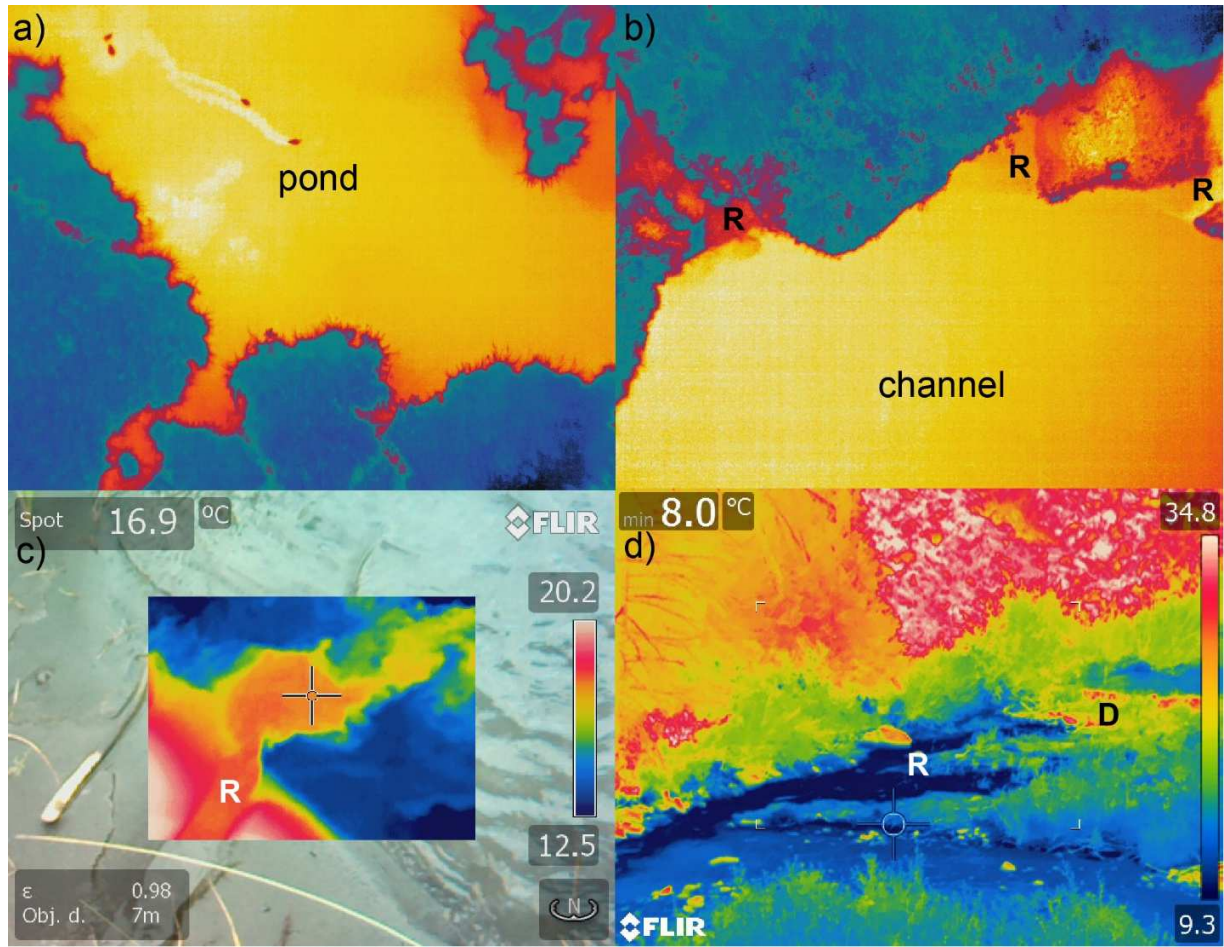
853 channel, while beaver pond return flow seeps (R) are typically warmer and lower in oxygen in
854 summer (panel e).

855



856

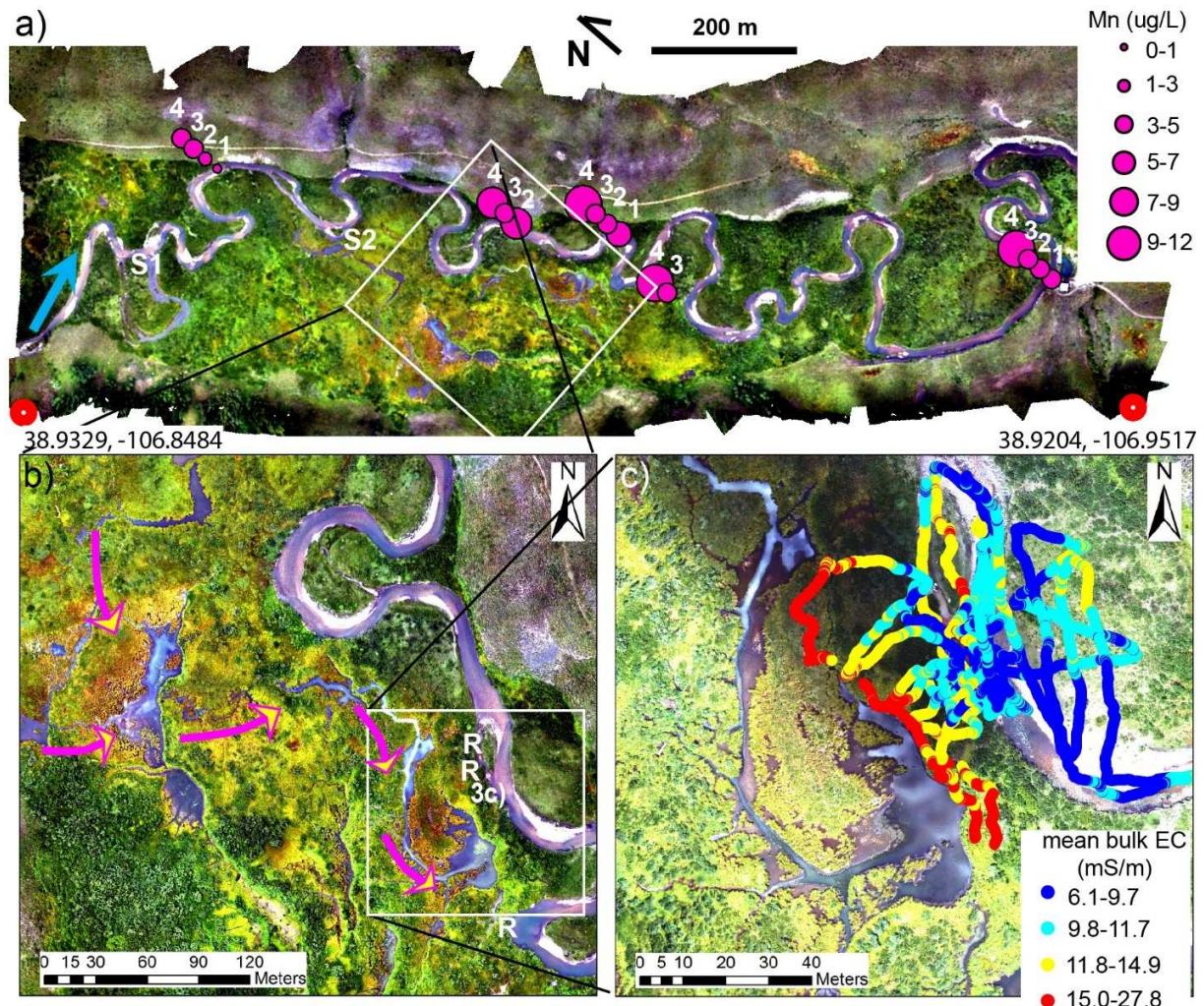
857 Figure 2. The 6-day mean and standard deviation of temperature along the East River fiber-optic
858 cable showing influence of ‘shunt’ beaver dam construction (S) and shallow, warm beaver pond
859 return flow seepage (R).



860

861 Figure 3. Thermal infrared imaging collected by drone of floodplain beaver ponds show
 862 relatively warm ponded areas, indicating by the hot colors in panel a), and beaver pond return
 863 flow seepage is shown by relative color scale in panel b), and close up through handheld imaging
 864 in panel c). Hillslope springs captured by floodplain beaver ponds collect relatively cold, deeper
 865 groundwater that discharges to the main channel after mixing with floodplain water (panel (d)).

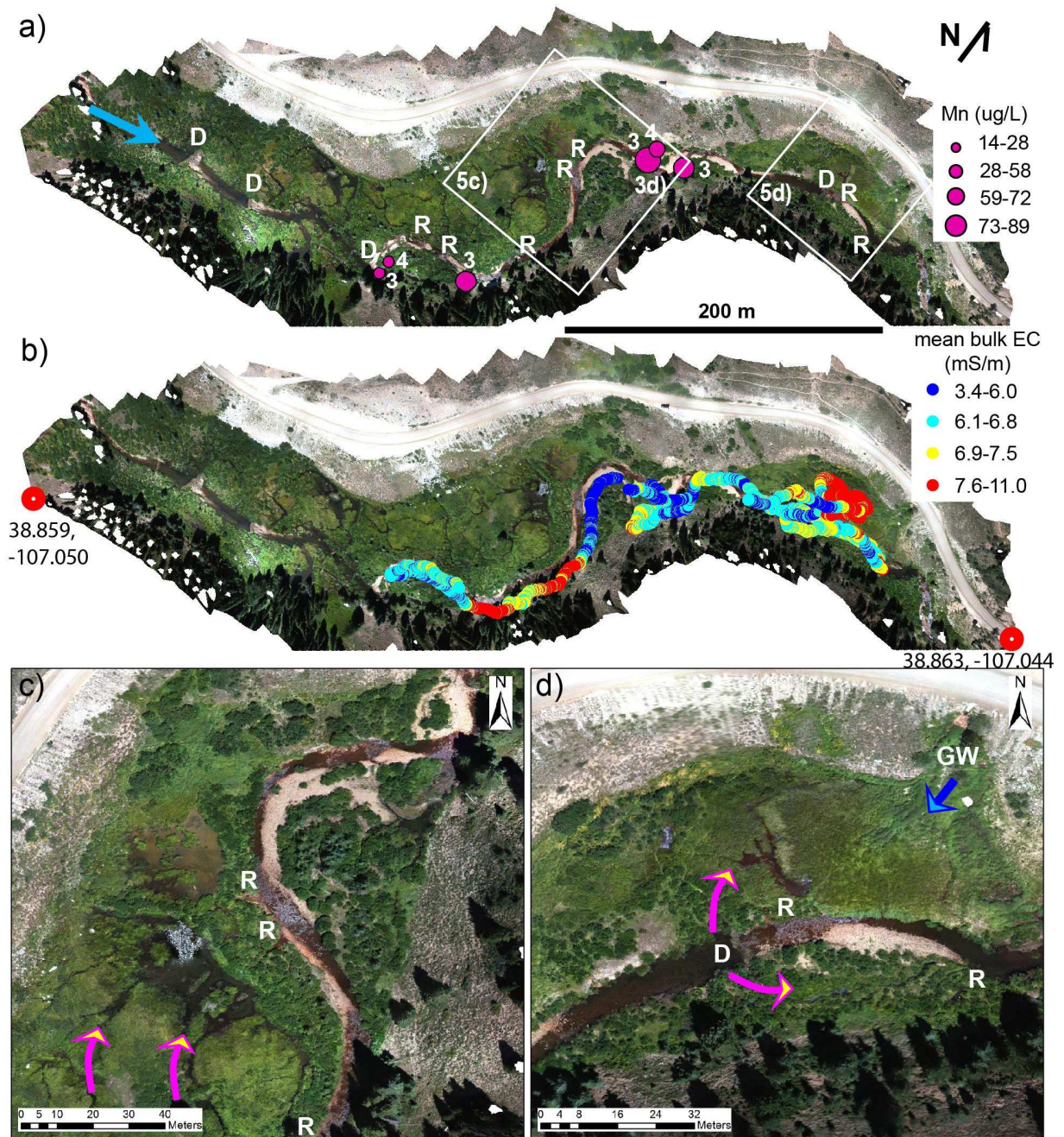
866



867

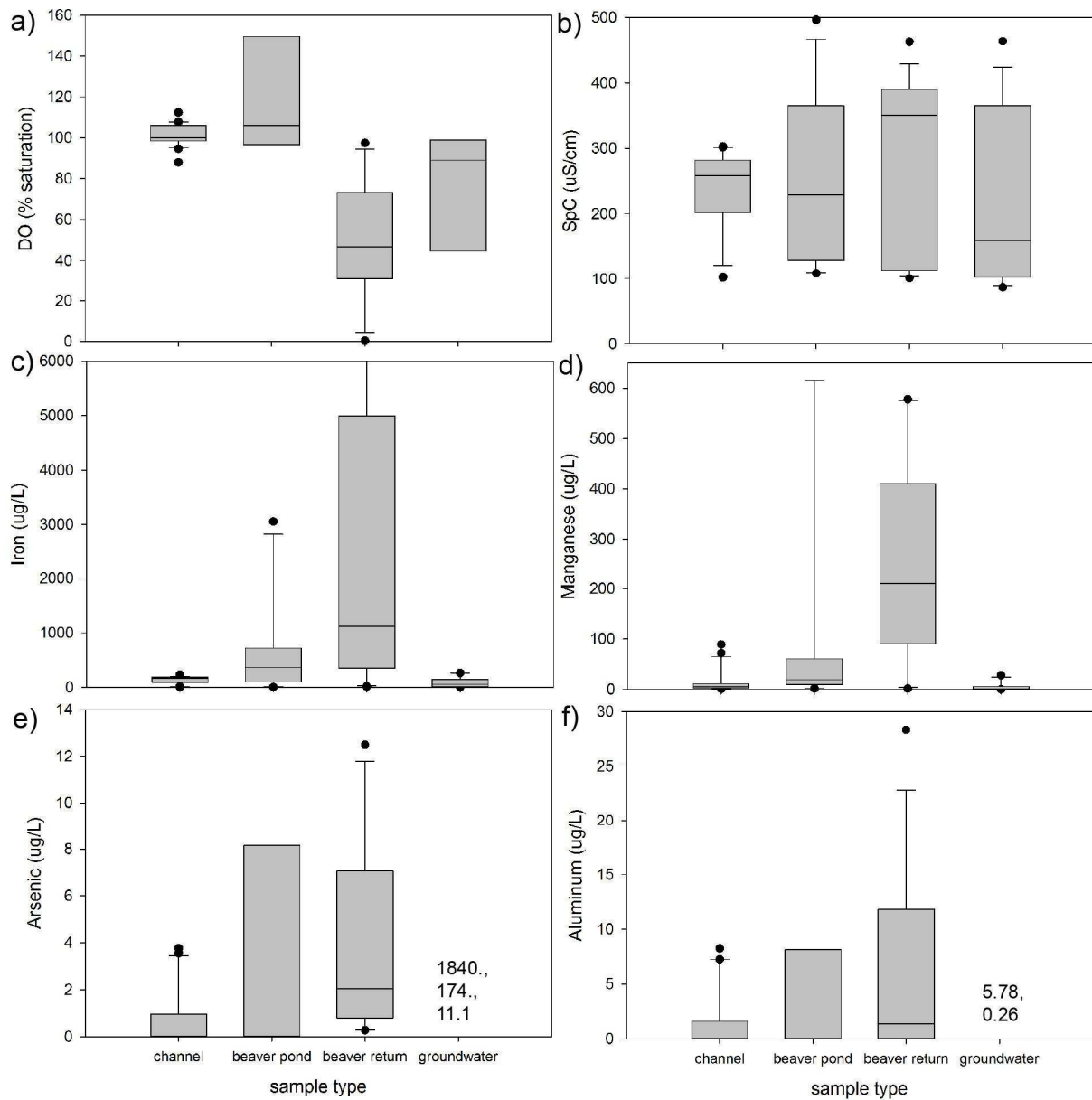
868 Figure 4. Panel a) displays the full size orthomosaic generated from 2017 drone imagery
 869 collected along the East River beaver impacted reach (north direction rotated left). River flow is
 870 left to right, and the two main beaver shunts are marked (S1, S2) that push channel water onto
 871 the adjacent floodplain. Main river channel dissolved manganese concentrations are shown for
 872 samples collected on: 1. August 2017, 2. June 21, 2018, 3. July 30, 2018, and 4. September 23,
 873 2018. Panel b) shows an enlarged image of the 2017 imagery of the more prominent floodplain
 874 beaver ponds and major return flow seeps (R), including the approximate location of the infrared
 875 image of Figure 3c). General surface flow patterns are shown with yellow arrowheads as inferred

876 from fine, light colored sediment transport following a rain event. Panel c) is an enlarged image
 877 of the 2018 drone-based orthomosaic showing lower pond water levels. Electromagnetic imaging
 878 transects indicate shallow subsurface plumes of reduced water (higher bulk conductivity)
 879 extending from the ponded area toward the main channel.



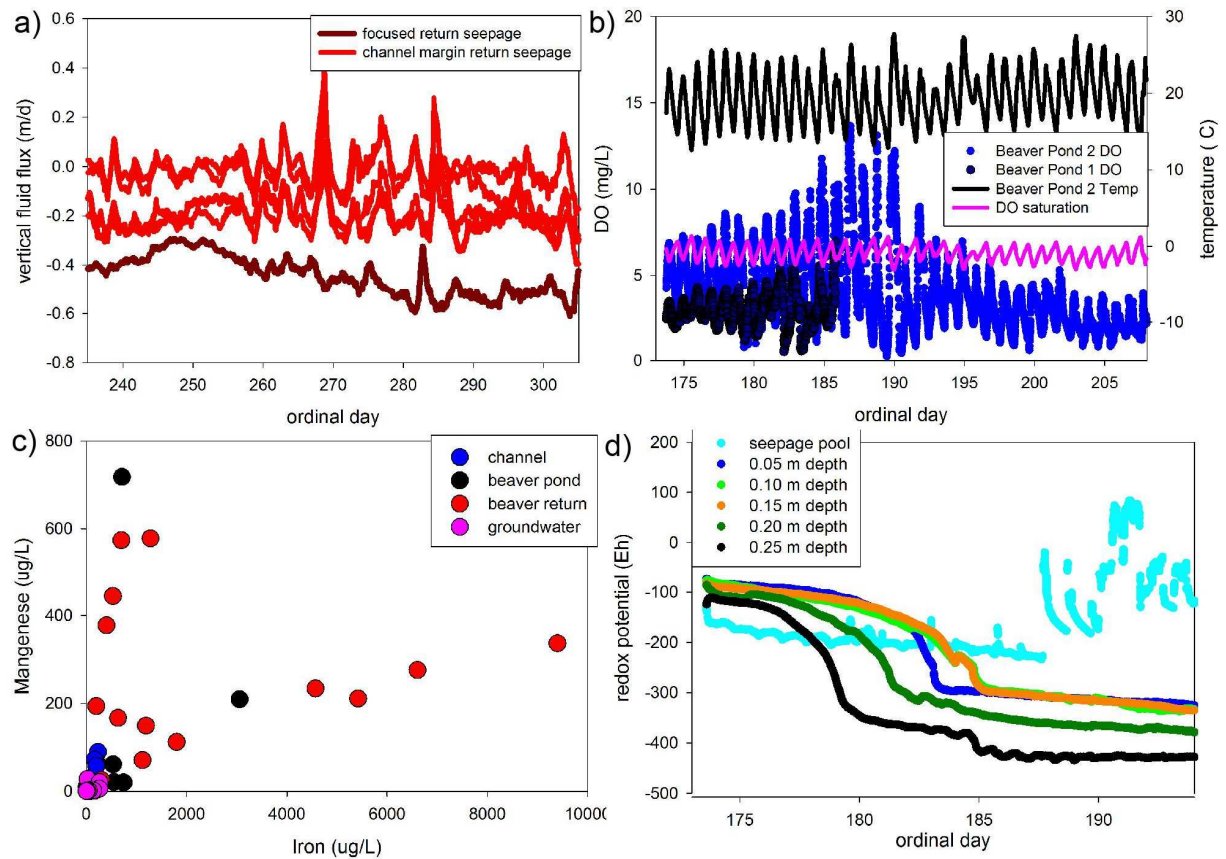
881 Figure 5. Panel a) shows the full orthomosaic generated from 2018 drone imaging collected
882 along the Coal Creek beaver impacted reach. Stream flow is left to right and channel spanning
883 beaver dams (D), return flows (R), and the locations of Figure panels 3d), 5c), and 5d) are
884 marked. Main channel dissolved manganese concentrations are shown for two sampling events
885 on: 3. August 2, 2018, and 4. September 25, 2018. Panel b) covers the same spatial extent as a),
886 and shows electromagnetic imaging transects data. Panel c) displays an enlarged view of the
887 larger floodplain ponds, and Panel d) shows a zoomed view of the most downstream channel
888 spanning dam and resulting floodplain diversions.

889



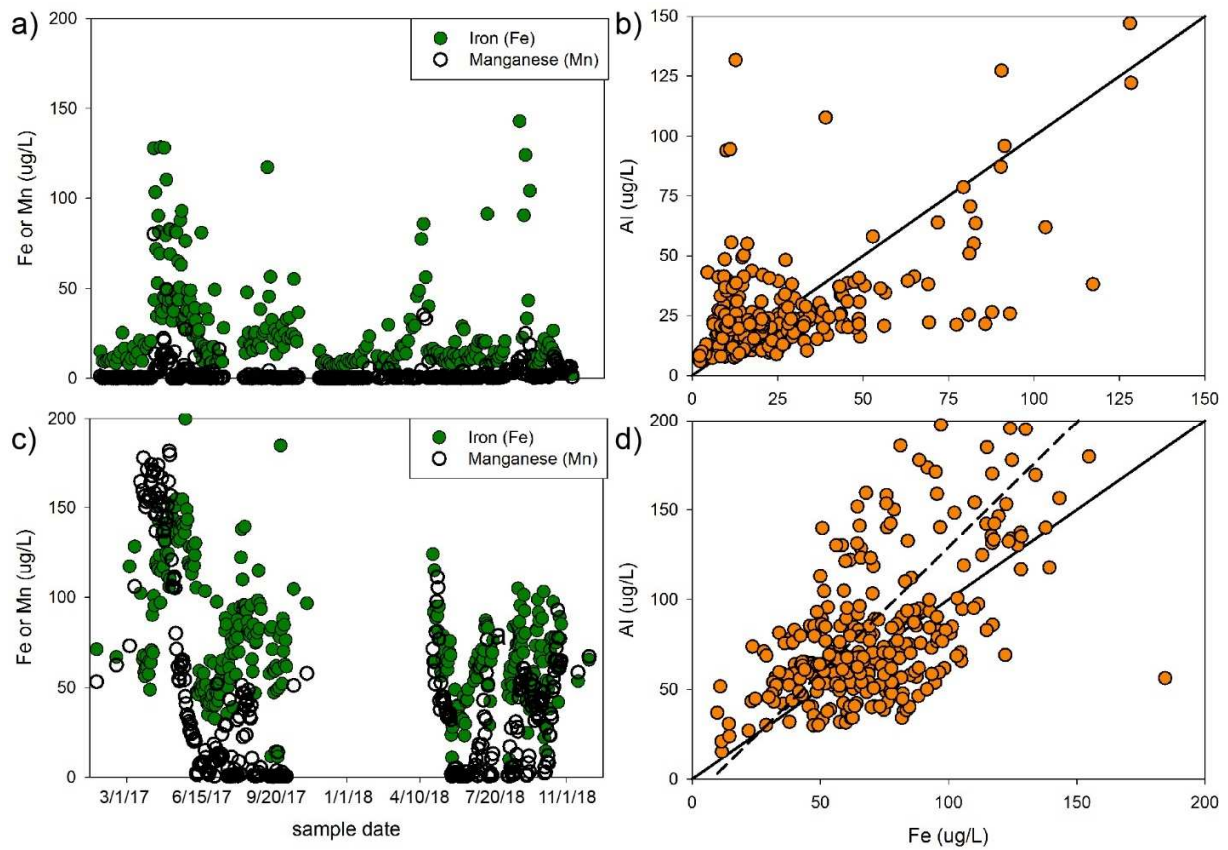
890

891 Figure 6. Water samples of source type: a) dissolved oxygen, b) specific conductivity, c) iron, d)
 892 manganese, e) arsenic, and f) aluminum. The vertical box indicates the interquartile range and
 893 the dots are outliers. For plots e) and f) all groundwater samples were below the respective
 894 detection limits except for the discrete values listed. The full chemical dataset is listed by sample
 895 in the Supplemental Material.



896

897 Figure 7. Panel a) displays summer/fall 2017 vertical return flow seepage rates, while panel b)
 898 shows measured dissolved oxygen (DO), temperature, and theoretical oxygen saturation for East
 899 River beaver ponds. Panel c) shows a plot of dissolved iron vs. manganese for all water samples
 900 of varied type; a sample of 14260.0 $\mu\text{g/L}$ Fe and 472.5 $\mu\text{g/L}$ Mn collected at the same location of
 901 the redox profile is not displayed. Panel d) displays multi-depth redox potential (Eh) monitored
 902 directly at the discharge point over time at a major East River return flow seep (shown in Figure
 903 3b).



904

905 Figure 8. Time series of iron, manganese, and aluminum collected over 2017-2018 1 km
 906 downstream of the distal end of the East River (panels a,b) and Coal Creek (panels b,c) beaver-
 907 impacted reaches. The solid line in panels b) and d) indicates a 1:1 relation while the dashed line
 908 in panel d) indicates the best linear fit to the data ($R^2=0.52$), no significant linear relation was
 909 found for the data in panel b).